AIP ADVANCES **3**, 102129 (2013)

Aperture-based antihydrogen gravity experiment: Parallel plate geometry

J. R. Rocha, R. M. Hedlof, and C. A. Ordonez[a]
Department of Physics, University of North Texas, Denton, Texas 76203, USA

(Received 12 September 2013; accepted 16 October 2013; published online 24 October 2013)

An analytical model and a Monte Carlo simulation are presented of an experiment that could be used to determine the direction of the acceleration of antihydrogen due to gravity. The experiment would rely on methods developed by existing antihydrogen research collaborations. The configuration consists of two circular, parallel plates that have an axis of symmetry directed away from the center of the earth. The plates are separated by a small vertical distance, and include one or more pairs of circular barriers that protrude from the upper and lower plates, thereby forming an aperture between the plates. Antihydrogen annihilations that occur just beyond each barrier, within a "shadow" region, are asymmetric on the upper plate relative to the lower plate. The probability for such annihilations is determined for a point, line and spheroidal source of antihydrogen. The production of 100,000 antiatoms is predicted to be necessary for the aperture-based experiment to indicate the direction of free fall acceleration of antimatter, provided that antihydrogen is produced within a sufficiently small antiproton plasma at a temperature of 4 K. [http://dx.doi.org/10.1063/1.4827498]

I. INTRODUCTION

There has never been reported experimental evidence that indicates the direction of the acceleration of antimatter (e.g., antiprotons, positrons, antihydrogen) due to a gravitational field. Experimental collaborations located at CERN such as ALPHA,[1–4] ATRAP,[5–7] ASACUSA,[8,9] AEGIS[10] and GBAR[11] are developing methods to study the properties of antihydrogen. These groups may pursue determining the direction antihydrogen falls in the presence of earth's gravitational field. Antihydrogen research may ultimately provide experimental tests of CPT (charge conjugation, parity, time reversal) symmetry and the weak equivalence principle of general relativity.[12–17]

Aperture-based antihydrogen gravity experiments have been previously considered that use a horizontal, cylindrical drift tube with a single or multiple aperture setup.[18,19] The present work represents a third iteration of study on a possible aperture-based antimatter gravity experiment. The analysis indicates that a substantial reduction in experimental run time may be possible relative to that predicted by the previous studies. The main objective of the experiment would be to determine whether antihydrogen accelerates vertically up or down as a result of earth's gravity. It is assumed that a detector, such as that used by the ALPHA collaboration,[2] would be used to distinguish between antihydrogen annihilations and cosmic rays.

Conceptual illustrations of the experimental setup are shown in Figs. 1 and 2. The configuration consists of two circular, parallel plates with the source of antihydrogen located within a region near the geometric center. The plates have an axis of symmetry directed away from the center of the earth and are separated by a small vertical distance. Between the plates, there are circular barriers that protrude from the top and bottom plates. Each circular barrier is coaxial with the axis of symmetry of the configuration.

[a]Author to whom correspondence should be addressed. Electronic mail: cao@unt.edu.

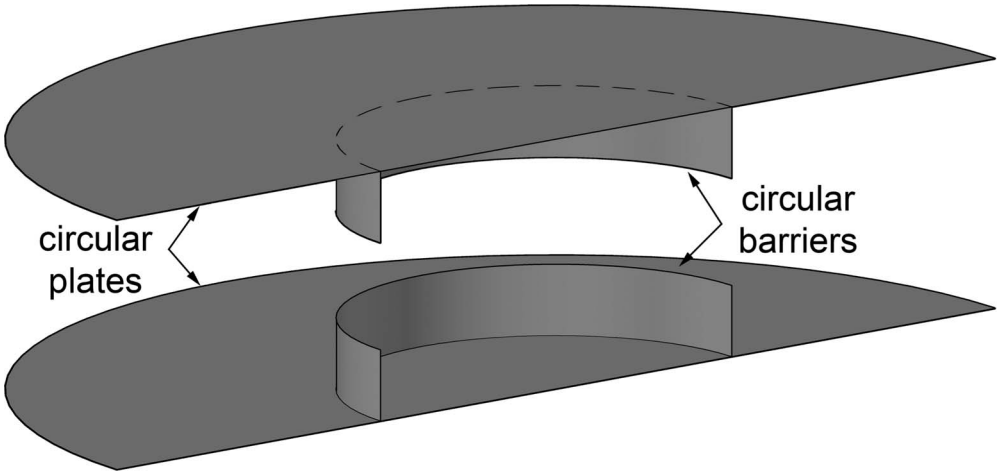

FIG. 1. Cross-sectional perspective view of the parallel plate apparatus.

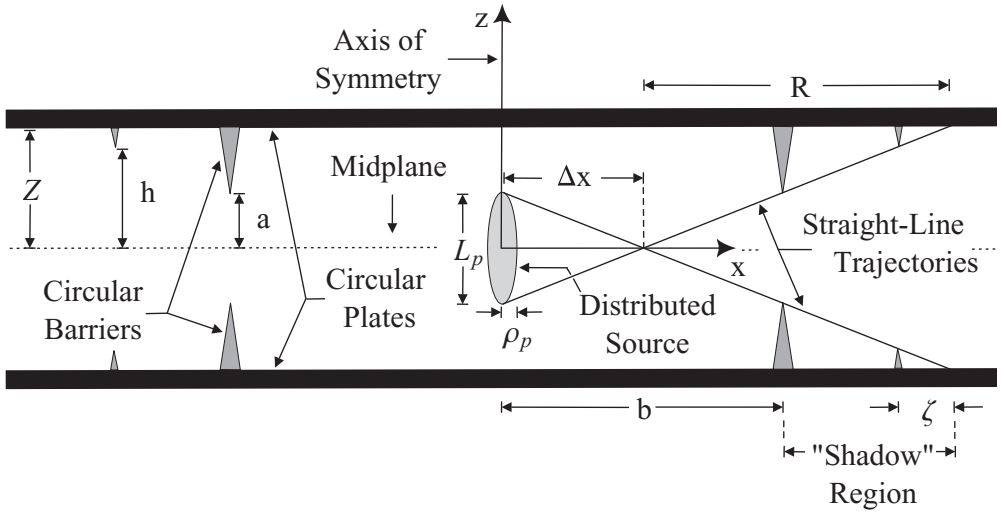

FIG. 2. Two-dimensional conceptual illustration of a parallel plate geometry for an antihydrogen gravity experiment.

The antiatoms are considered to have initial coordinates within the distributed source shown in Fig. 2. The two straight line trajectories, passing infinitesimally close to the edges of the upper and lower barriers, define two "shadow" regions on the upper and lower plates, respectively. Provided no other forces act on the antiatoms, annihilations within the shadow regions are only possible if the trajectories of the antiatoms are affected by gravity. If antimatter accelerates towards the earth, only annihilations within the shadow region of the lower plate would be possible. If antimatter accelerates away from the earth, only annihilations within the shadow region of the upper plate would be possible. In Sec. II, an analytical model is presented for the parallel plate configuration considering a point source of antiatoms. A Monte Carlo simulation is presented that considers either a point source of antiatoms (Sec. III) or a spatially distributed source of antiatoms (Sec. IV). A discussion and concluding remarks are presented in Sec. V.

II. ANALYTICAL MODEL

A Cartesian coordinate system with coordinates (x, y, z) and associated unit vectors ($\hat{\boldsymbol{i}}$, $\hat{\boldsymbol{j}}$, $\hat{\boldsymbol{k}}$) is defined such that the axis of symmetry coincides with the z-axis, and the coordinate origin is located at the point where the axis of symmetry intersects the midplane between the plates. Suppose

that antimatter experiences a gravitational acceleration that is equal in magnitude and opposite in direction to that of ordinary matter. An antiatom's acceleration due to gravity is expressed as $\boldsymbol{g} = g\hat{\boldsymbol{k}}$, where g is the associated magnitude. The equations of motion in Cartesian coordinates are

$$\begin{aligned} x(t) &= x_0 + v_{0x}t, \\ y(t) &= y_0 + v_{0y}t, \\ z(t) &= z_0 + v_{0z}t + \frac{1}{2}gt^2. \end{aligned} \tag{1}$$

Here, $x(t)$, $y(t)$ and $z(t)$ are the displacements relative to the coordinate origin at a time t, x_0, y_0 and z_0 are the initial coordinates, and v_{0x}, v_{0y} and v_{0z} are the components of the initial velocity of the antiatom. To develop an analytical model, it is assumed that an antiatom's initial position is located at the coordinate origin such that $x_0 = y_0 = z_0 = 0$. In terms of spherical coordinates, the initial velocity components are written as

$$\begin{aligned} v_{0x} &= v_0 \sin(\theta_0)\cos(\phi_0), \\ v_{0y} &= v_0 \sin(\theta_0)\sin(\phi_0), \\ v_{0z} &= v_0 \cos(\theta_0), \end{aligned} \tag{2}$$

where v_0 is the initial speed of an antiatom, and θ_0 and ϕ_0 are the angles that describe the initial direction of motion for the antiatom. Due to the azimuthal symmetry of the system, the problem may be solved in the r-z plane of a cylindrical coordinate system using radial r and axial z coordinates, with no loss of generality. The radial coordinate r is expressed in terms of the Cartesian coordinates by $r^2(t) = x^2(t) + y^2(t)$. Solving for time gives $t = r/[v_0 \sin(\theta_0)]$. The initial speed of an antiatom may be expressed in terms of initial kinetic energy K_0 as $v_0 = \sqrt{2K_0/m}$, where m is the mass of an antiatom. Substitution and rearrangement gives

$$K_0 = \frac{mgr^2}{4[z - r\cot(\theta_0)]\sin^2(\theta_0)}. \tag{3}$$

There exists a range of initial kinetic energies K_0 and angles θ_0 that result in a trajectory that intersects the shadow region of the upper plate. A lower bound on the initial kinetic energy coincides with a trajectory that passes infinitesimally close to the lower edge of the upper barrier located at $z = a$ and $r = b = \frac{aR}{Z}$. Here, a is the vertical distance from the midplane to the lower edge of the upper barrier, R is the radial distance from the point source of antiatoms to the far edge of the shadow region, b is the radial distance from the z-axis to the circular barriers, and Z is the vertical distance from the midplane to the upper plate. (See Fig. 2, but with distributed source parameters, defined later, having the values $\Delta x = L_p = \rho_p = 0$.) Substitution into Eq. (3) yields the minimum initial kinetic energy for an antiatom to reach the shadow region of the upper plate,

$$K_{0,\min} = \frac{mgR^2}{4(Z/a)[Z - R\cot(\theta_0)]\sin^2(\theta_0)}. \tag{4}$$

Likewise, an upper bound on the initial kinetic energy corresponds to a trajectory that intersects the upper plate at the far edge of the shadow region, i.e., at $z = Z$ and $r = R$. Substitution into Eq. (3) provides the maximum initial kinetic energy,

$$K_{0,\max} = \frac{mgR^2}{4[Z - R\cot(\theta_0)]\sin^2(\theta_0)}. \tag{5}$$

For the analytical model, the lower and upper bounds on the initial angle are considered to be those corresponding to the straight line trajectories in Fig. 2 (with $\Delta x = 0$),

$$\theta_{0,\min} = \arctan\left(\frac{R}{Z}\right), \tag{6}$$

and

$$\theta_{0,\max} = \pi - \arctan\left(\frac{R}{Z}\right). \tag{7}$$

An annihilation distribution that is maximally asymmetric between the upper and lower plates corresponds to one associated with the maximum probability for the initial kinetic energy and angle to satisfy $K_{0,\,\min} < K_0 < K_{0,\,\max}$ and $\theta_{0,\,\min} < \theta_0 < \theta_{0,\,\max}$. The probability for an antiatom's initial motion to satisfy $K_{0,\,\min} < K_0 < K_{0,\,\max}$ and $\theta_{0,\,\min} < \theta_0 < \theta_{0,\,\max}$ is evaluated by assuming that the antiatoms have a Maxwellian velocity distribution. Such an assumption is consistent with producing antiatoms within a thermalized, drifting (e.g., rotating) plasma, provided that the antiproton drift speed is much smaller than the antiproton thermal speed throughout the plasma. The probability density function in terms of Cartesian initial velocity components is given by

$$f_c(\boldsymbol{v_0}) = f_0 \exp\left[-\frac{m(v_{0x}^2 + v_{0y}^2 + v_{0z}^2)}{2k_B T}\right], \tag{8}$$

where $\boldsymbol{v_0}$ represents the initial Cartesian velocity components v_{0x}, v_{0y} and v_{0z}, f_0 is a normalization constant, k_B is Boltzmann's constant and T is temperature.

A change of variables is carried out to write the probability density in spherical coordinates (v_0, θ_0, ϕ_0). In spherical coordinates, velocity space is defined to have the following ranges: $0 \le v_0 < \infty$, $0 \le \theta_0 \le \pi$ and $0 \le \phi_0 < 2\pi$. Recognizing that $v_0^2 = v_{0x}^2 + v_{0y}^2 + v_{0z}^2$ and employing the Jacobian transformation matrix, the normalized velocity-space probability density in spherical coordinates is given by

$$f_s(v_0, \theta_0) = \frac{1}{\sqrt{2\pi}} \left(\frac{m}{k_B T}\right)^{3/2} v_0^2 \, \sin(\theta_0) \exp\left[-\frac{m\, v_0^2}{2k_B T}\right]. \tag{9}$$

Another change of variables is done to write the probability density in terms of $K_0 = \frac{1}{2} m v_0^2$ and θ_0. The normalized probability density is then

$$f(K_0, \theta_0) = \frac{1}{\sqrt{\pi (k_B T)^3}} \, \sin(\theta_0) \sqrt{K_0} \exp\left[-\frac{K_0}{k_B T}\right]. \tag{10}$$

Thus, the probability, P, for an antiatom to satisfy the conditions $K_{0,\,\min} < K_0 < K_{0,\,\max}$ and $\theta_{0,\,\min} < \theta_0 < \theta_{0,\,\max}$ is

$$P = \int_{\theta_{0,\min}}^{\theta_{0,\max}} \int_{K_{0,\min}}^{K_{0,\max}} f(K_0, \theta_0)\, dK_0 d\theta_0. \tag{11}$$

The inner integral can be evaluated analytically. The definite integral is

$$\int_{K_{0,\min}}^{K_{0,\max}} f(K_0, \theta_0)\, dK_0 = \left[\frac{1}{2} \operatorname{erf}\left(\sqrt{\frac{K_0}{k_B T}}\right) - \sqrt{\frac{K_0}{\pi k_B T}} \exp\left(-\frac{K_0}{k_B T}\right)\right] \sin(\theta_0) \Bigg|_{K_{0,\min}}^{K_{0,\max}}, \tag{12}$$

where erf is the error function. The outer integral in Eq. (11) is evaluated numerically.

A maximized value for P corresponds to an annihilation distribution that is maximally asymmetric between top and bottom plates. The distance from the midplane to the barrier edge is written as $a = Z/\kappa$, where κ must be larger than one. Figure 3 shows the effect on P of changing one parameter and holding the others constant. For the parameters considered, the plots indicate that P decreases nonlinearly with T, increases linearly with R and increases nearly linearly with κ. For the given values of T, R and κ, P has a maximum value at a single value for Z.

A temperature of $T = 4$ K is assumed based on the ATRAP collaboration's reported achievement of cooling an antiproton plasma to a temperature of $T = 3.5$ K.[5] The radius of the plates is chosen to be $R = 0.6$ m, considering space limitations for the experimental apparatus. The aperture size a and barrier location b are related by $b = (aR)/Z = R/\kappa$. Thus, a smaller value for a is associated with circular barriers that are necessarily closer to the antihydrogen source for fixed Z in the present model. A value of $\kappa = 10$ is chosen, and the probability is found to have a maximum at $Z = 0.0501$ m.

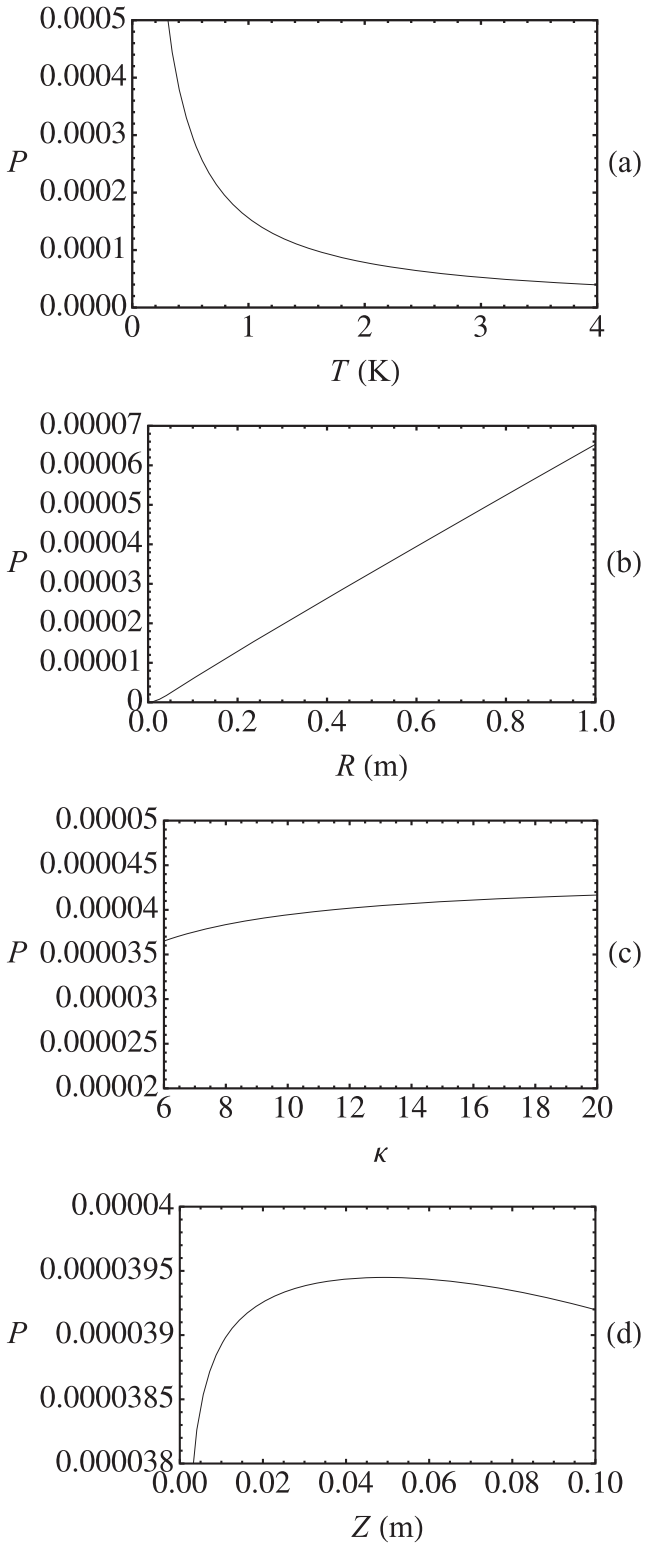

FIG. 3. Effect of changing a single parameter, (a) T, (b) R, (c) κ or (d) Z. The values of parameters that are held constant are $T = 4$ K, $R = 60$ cm, $\kappa = 10$, and $Z = 5.01$ cm.

A base case is defined with parameters $T = 4$ K, $R = 0.6$ m, $\kappa = 10$ and $Z = 0.0501$ m, which gives a maximum value of $P = 3.945 \times 10^{-5}$. Thus, for every 10^6 antiatoms produced, the model predicts that there should be 39 annihilations within the shadow region. It should be noted that the ALPHA collaboration reported producing antihydrogen within a thermalized antihydrogen plasma having a temperature $T \approx 54$ K.[2] For this temperature, with the same values for R and κ as in the base case, it is found that the value $Z = 0.0292$ m gives a maximum value of $P = 2.95 \times 10^{-6}$. The model then predicts approximately 3 annihilations within the shadow region for every 10^6 antiatoms produced. Another calculation is also provided, by way of example, for the base case parameters, except with $Z = 0.08$ m and $\kappa = 4$. It is found that $P = 3.276 \times 10^{-5}$, predicting 33 annihilations within the shadow region for every 10^6 antiatoms produced.

III. MONTE CARLO SIMULATION

A Monte Carlo simulation is used to determine the effect of having a distributed source of antiatoms. For the first set of simulations, however, each antiatom's trajectory is considered to start from a point at the coordinate origin,

$$x_0 = 0$$
$$y_0 = 0$$
$$z_0 = 0. \tag{13}$$

The antiatom's initial Cartesian velocity components are given by Eq. (2). The velocity-space probability density, Eq. (9), is sampled to obtain values for v_0, θ_0 and ϕ_0. Since Eq. (9) has no dependence on the azimuthal angle, ϕ_0 is sampled using

$$\phi_0 = 2\pi R_\phi, \tag{14}$$

where R_ϕ denotes a random number between 0 and 1. For the remainder of this work, R with a subscript attached will be used to distinguish between different random numbers equally likely to have any value between 0 and 1.

The part of the probability density in Eq. (9) that involves θ_0 is separable and is proportional to $\sin(\theta_0)$. To reduce the computation time, θ_0 is sampled over the range $\theta_l < \theta_0 < \theta_u$, where θ_l and θ_u represent lower and upper limits on sampled values. The lower limit is chosen to be the angle associated with straight-line trajectories that pass infinitesimally close to the lower edge of the upper barrier, $\theta_l = \theta_{0,\min} = \arctan(R/Z)$. The upper limit is chosen to be the angle associated with straight-line trajectories that pass infinitesimally close to the upper edge of the lower barrier, $\theta_u = \theta_{0,\max} = \pi - \arctan(R/Z)$. The sampling expression is given by

$$R_\theta = \frac{\int_{\theta_l}^{\theta_0} \sin\theta \, d\theta}{\int_{\theta_l}^{\theta_u} \sin\theta \, d\theta}. \tag{15}$$

Solving for θ_0 gives

$$\theta_0 = \arccos\left(\frac{1 - 2R_\theta}{\sqrt{1 + \frac{R^2}{Z^2}}}\right). \tag{16}$$

The fraction of the solid angle that is sampled is

$$F_\Omega = \frac{\int_{\theta_l}^{\theta_u} \sin\theta \, d\theta}{\int_0^{\pi} \sin\theta \, d\theta} = \frac{1}{\sqrt{1 + \frac{R^2}{Z^2}}}. \tag{17}$$

The initial speed of an antiatom is calculated as $v_0 = \sqrt{v_x^2 + v_y^2 + v_z^2}$, where v_x, v_y and v_z are sampled using a Maxwellian distribution with a zero mean and a standard deviation given by the thermal speed, $v_t = \sqrt{(kT)/m}$. The equations of motion are given by Eq. (1), with an assumed upward acceleration given by $\boldsymbol{g} = g\hat{\boldsymbol{k}}$.

TABLE I. Summary of results for the Monte Carlo simulations for the point and line antihydrogen sources. All simulations are run with $R = 0.6$ m and $N = 10^7$. The value of P is calculated using Eq. (11), which is not applicable (NA) for finite values of L_p.

$\langle N_{\bar{H}} \rangle \pm SD$	$\frac{\langle N_{\bar{H}} \rangle}{(P \cdot N)} \pm \frac{SD}{(P \cdot N)}$	T (K)	Z (m)	κ	a (m)	L_p (m)	N_s
383.5 ± 20.8	0.972 ± 0.053	4	0.0501	10	0.00501	0	832,104
28.9 ± 5.3	0.978 ± 0.179	54	0.0292	10	0.0029	0	486,091
323.2 ± 21.0	0.987 ± 0.064	4	0.08	4	0.02	0	1,321,637
28.3 ± 5.5	NA	4	0.0501	10	0.00501	0.0008	832,104
12.1 ± 3.5	NA	4	0.0501	10	0.00501	0.004	832,104
9.9 ± 3.1	NA	4	0.0501	10	0.00501	0.008	832,104
8.2 ± 2.3	NA	4	0.0501	10	0.00501	0.01	832,104

Three conditions must be met for an antiatom to annihilate in the shadow region. (1) Prior to annihilation in the shadow region, the antiatom must remain in the space between the two plates. (2) The antiatom must pass through the aperture created by the upper and lower barriers. (3) The antiatom must intersect the upper or lower plate within the shadow region. To determine if these conditions are met, it is convenient to consider the coordinates of the antiatoms at two times throughout the trajectory. The first, τ_1, corresponds to the time at which the antiatom travels the radial distance to the barriers and is given by $\tau_1 = b/\sqrt{v_{0x}^2 + v_{0y}^2}$. The second, τ_a, corresponds to the time at which the antiatom annihilates on the upper or lower plates. Here, τ_1 and τ_a must be real and positive. The annihilation time is found by evaluating the equation of motion in the z direction in Eq. (1) at $t = \tau_a$ and $z(\tau_a) = |Z|$. Solving for τ_a yields four solutions. Of these, τ_a would take on the form of the solution that is real, positive and has the smallest value. If $\tau_a > \tau_1$ the trajectory satisfies condition (1). If $|z(\tau_1)| < a$, the antiatom passes through the aperture satisfying condition (2). If $b < \sqrt{x(\tau_a)^2 + y(\tau_a)^2} < R$ the trajectory satisfies condition (3). If all three conditions are met, the coordinates of the simulated annihilation site is recorded.

Let N_s, $N = \frac{N_s}{F_\Omega}$ and $N_{\bar{H}}$ denote the number of simulated antiatoms, the equivalent number of antiatoms that would be emitted into the entire 4π solid angle and the number of simulated annihilations that occur within the shadow region on the upper plate, respectively. One simulation, carried out with a specified parameter set (e.g., a set of values for R, T, Z, a and N_s), yields a single value for $N_{\bar{H}}$. Twenty simulations are carried out with $N = 10^7$ for each set of parameters, and the average $\langle N_{\bar{H}} \rangle$ and standard deviation SD are recorded. The results are shown in Table I. The correlation between statistical results for $N_{\bar{H}}$ and the probability evaluated using Eq. (11) is shown by evaluating the quotients $\langle N_{\bar{H}} \rangle / (PN)$ and $SD/(PN)$. A value $\langle N_{\bar{H}} \rangle / (PN) = 1$ would indicate the best possible agreement between the analytical model and the Monte Carlo simulation. For the base case, an average of 383.5 ± 20.8 simulated annihilations occur within the shadow region. For $T = 54$ K, $Z = 0.0292$ m, and the same values for R and κ as in the base case, an average of 28.9 $\pm$ 5.3 simulated annihilations occur within the shadow region. The simulation is also run for the parameter set $T = 4$ K, $Z = 0.08$ m and $\kappa = 4$. An average of 323.2 ± 21.0 annihilations occur within the shadow region.

Figure 4 shows the trajectories of antiatoms that annihilate in the shadow region for parameters $R = 0.6$ m, $Z = 0.0493$ m, $\kappa = 10$ and $N = 100{,}000$ at temperatures 54 K, 4 K and 0.4 K. The initial conditions for Fig. 4 are sampled in the same way as those for the first three rows of Table I, i.e., by using Eqs. (13), (14), and (16) and a sampled Maxwellian speed distribution. The effect of gravity on the trajectories is more pronounced at lower temperatures.

The ALPHA collaboration reported the production of 6×10^3 antiatoms for each bunch of antiprotons delivered by the CERN Antiproton Decelerator (AD).[2] While the AD was in operation, the bunches were provided approximately every 100 seconds. With full utilization of the bunches taken as an upper limit, the antiatom production rate would be about 60 antiatoms per second. It is illustrative to consider such a production rate here, even though the configuration considered here does not employ a horizontal cylindrical drift tube, which would be more compatible with the

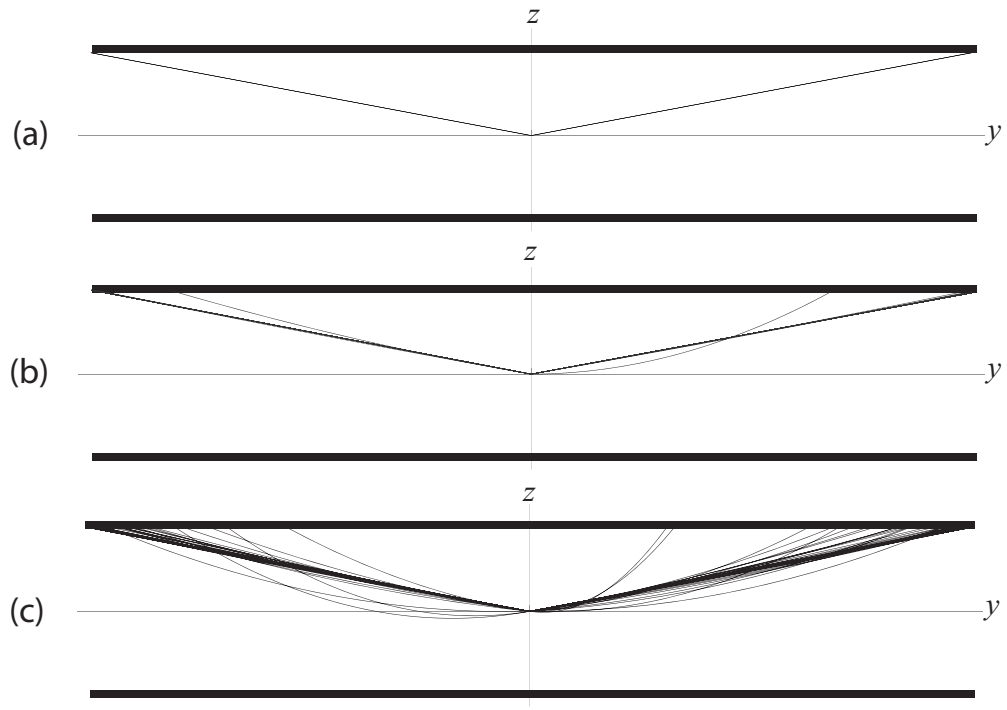

FIG. 4. Trajectories are shown for antiatoms that originate at the coordinate origin and annihilate in the shadow region out of $N_s = 8{,}190$ simulated antiatoms with parameters $R = 0.6$ m, $Z = 0.0493$ m and $\kappa = 10$. In order to show trajectories in the y-z plane only, $\phi_0 = \pi/2$ and $\phi_0 = 3\pi/2$ were used. The temperatures for (a), (b) and (c) are 54 K, 4 K and 0.4 K, respectively. In (a), four (4) annihilations occur. The associated four trajectories start at the coordinate origin, with two pairs of trajectories that overlap and are indistinguishable. The number of annihilations in the shadow region tends to increase with decreasing temperature (4 at 54 K, 37 at 4 K and 376 at 0.4 K). At higher temperatures, trajectories tend to follow nearly straight paths.

ALPHA apparatus. For $T = 4$ K, the results obtained here indicate that it would only be necessary to produce about 10^5 antiatoms for the experiment to indicate the direction of free fall acceleration, provided that antihydrogen is produced within a sufficiently small antihydrogen plasma. This could be achieved in a minimum of about 30 minutes of experimental run time. This corresponds to a reduction in experimental run time by a factor of 3,000 from the 58 days that was previously reported in Ref. 18 for an aperture-based experiment that employs a cylindrical drift tube.

IV. EFFECT OF A SPATIAL DISTRIBUTION OF INITIAL COORDINATES

The effects of having two different spatial distributions of initial coordinates for the antihydrogen atoms are evaluated. The first is an infinitesimally thin line source with finite length L_p oriented vertically along the axis of symmetry of the apparatus and centered about the midplane between the plates. In this case, the azimuthal symmetry of the source distribution and the apparatus allow for the simulation to be carried out in two dimensions with no loss of generality. The x-z plane is chosen. The shadow region is defined by two straight line trajectories that start from the axis of symmetry at the locations $z = \pm L_p/2$ and that pass infinitesimally close to the barriers, as shown in Fig. 2. The origin is displaced by an amount Δx. Physically, Δx represents the radial distance from the axis of symmetry to the point at which the two straight line trajectories intersect the midplane. Here, $\Delta x = \frac{L_p}{2} \tan\theta_l$, where $\theta_l = \arctan\left(\frac{R}{Z}\right)$, and R is now the radial distance from the point at which the two straight line trajectories intersect the midplane to the far edge of the shadow region. Thus,

$$\Delta x = \frac{RL_p}{2Z}. \tag{18}$$

The initial coordinates are sampled via

$$x_0 = -\frac{RL_p}{2Z}$$
$$z_0 = \eta_z \frac{L_p}{2}. \tag{19}$$

Here and hereafter, η_z will denote a random real number equally likely to have any value between -1 and 1. Restricting the motion of the antiatoms to two dimensions and displacing the origin in such a manner allows for the implementation of the sampling expression for θ_0 given in Eq. (16). The sampling expressions for the components of the initial velocity are

$$v_{0x} = v_0 \sin(\theta_0),$$
$$v_{0z} = v_0 \cos(\theta_0). \tag{20}$$

The simulation is carried out for $N = 10^7$ and $N_s = F_\Omega N = 832,104$ for the base case parameters at different source lengths, and the results are shown in Table I. It is found that the number of annihilations within the shadow region decreases significantly from an average of 383.5 ± 20.8 for the point source to 28.3 ± 5.5 for a source with length 0.8 mm, 12.1 ± 3.5 for $L_p = 4$ mm, 9.9 ± 3.1 for $L_p = 8$ mm and 8.2 ± 2.3 for $L_p = 1$ cm. The simulated data indicates that as L_p is increased, the total number of annihilations in the shadow region is decreased. It should be noted that, due to the offset of the origin from the axis of symmetry of the plates, the radius of the plates would now have a radius $r_{plates} = R + \Delta x$.

The second source distribution is a spheroid of equatorial radius ρ_p and polar radius $\frac{L_p}{2}$ centered about the origin. The spheroid is oriented such that the polar radius coincides with the z-axis and the equatorial radius lies in the x-y plane. The sampling expression used for the initial Cartesian coordinates of antiatoms within the spheroid are

$$x_0 = \rho_p \sqrt{R_r\left(1 - \eta_z^2\right)} \cos(2\pi R_\phi),$$
$$y_0 = \rho_p \sqrt{R_r\left(1 - \eta_z^2\right)} \sin(2\pi R_\phi),$$
$$z_0 = \eta_z \frac{L_p}{2}. \tag{21}$$

These expressions are arrived at as indicated in the Appendix.

The antiatoms' initial coordinates are sampled using Eq. (21), and the equations of motion are given by Eq. (1). The Cartesian velocity components are written in the form of Eq. (2). The magnitude is given by $v_0 = \sqrt{v_x^2 + v_y^2 + v_z^2}$, where v_x, v_y and v_z are sampled as was done for the point source. For the spheroidal geometry it is necessary to sample the full solid angle. Therefore, $N = N_s = 10^7$ is used for all simulations. The sampling expression for ϕ_0 is $\phi_0 = 2\pi R_\phi$. The sampling expression for θ_0 is

$$\theta_0 = \arccos(1 - 2R_\theta), \tag{22}$$

which is found by solving

$$R_\theta = \frac{\int_0^{\theta_0} \sin\theta \, d\theta}{\int_0^{\pi} \sin\theta \, d\theta}. \tag{23}$$

The time at which the antiatom travels the radial distance to the barriers is given by solving $b^2 = x(\tau_1)^2 + y(\tau_1)^2$ for τ_1. If the conditions imposed in Sec. III are satisfied, then the coordinates at which the antiatom annihilates are recorded.

A summary of the results for the spheroidal source of antiatoms, using the base case parameters for $N = N_s = 10^7$ simulated antiatoms, is shown in Table II. The effects of changing the dimensions of the antihydrogen source is evaluated by carrying out the simulation for six different values for the equatorial radius, ρ_p, and three different values for the source length, L_p. The values for the

TABLE II. Summary of results for the Monte Carlo simulations with the spheroidal antihydrogen source. All simulations are run with $N = N_s = 10^7$, $T = 4$ K, $R = 0.6$ m, $Z = 5.01$ cm, $\kappa = 10$ and $a = 5.01$ mm.

$\langle N_{\bar{H}} \rangle \pm SD$	L_p (m)	ρ_p (m)
7.9 ± 3.4	0.01	0.00004
12.6 ± 2.7	0.004	0.00004
28.0 ± 4.7	0.001	0.00004
7.7 ± 2.3	0.01	0.00008
12.9 ± 2.7	0.004	0.00008
27.1 ± 4.5	0.001	0.00008
7.7 ± 2.8	0.01	0.0004
13.1 ± 3.6	0.004	0.0004
27.4 ± 6.1	0.001	0.0004
7.9 ± 2.3	0.01	0.0008
12.6 ± 2.8	0.004	0.0008
27.0 ± 4.9	0.001	0.0008
5.9 ± 2.3	0.01	0.004
11.8 ± 3.2	0.004	0.004
19.7 ± 4.6	0.001	0.004
8.2 ± 2.7	0.01	0.008
9.9 ± 3.6	0.004	0.008
17.1 ± 3.8	0.001	0.008

equatorial radius that were used were $\rho_p = 0.04$ mm, $\rho_p = 0.08$ mm, $\rho_p = 0.4$ mm, $\rho_p = 0.8$ mm, $\rho_p = 4$ mm and $\rho_p = 8$ mm. For each value of ρ_p the simulation is carried out for three source lengths, $L_p = 10$ mm, $L_p = 4$ mm and $L_p = 1$ mm. The simulated data indicates that the average number of annihilations, $\langle N_{\bar{H}} \rangle$, has little dependence on the value for the equatorial radius for the range of values considered. In contrast, a change in length of the source by a factor of 10 from $L_p = 10$ mm to $L_p = 1$ mm causes the value of $\langle N_{\bar{H}} \rangle$ to increase by more than a factor of three in some cases.

V. DISCUSSION AND CONCLUDING REMARKS

It should be noted that in this work the detection system implemented is assumed to be capable of precisely determining the site of annihilation. In reality, however, there will be a finite resolution for the detectors. For instance, in the ALPHA apparatus the axial resolution for diagnosing annihilation events is about 5 mm.[2] Two possible methods of resolving this problem could be: (1) Place particle detectors with higher resolution within the shadow region. (2) Place a secondary set of circular barriers a distance ζ, equal to the resolution of the detection system, from the edge of the shadow region as shown in Fig. 2. For example, if the resolution of the detectors is 5 mm then the barriers should be placed $\zeta = 5$ mm from the edge of the shadow region. The vertical distances, h, from the midplane to the edge of the secondary barriers would depend on the geometry of the antihydrogen source. For the point and line source distributions $h = Z(1 - \zeta/R)$. For the spheroidal source distribution, h may be found by evaluating Eq. (A11) at $z = -h$, $r = \Delta x + R - \zeta$, and solving for h. With the secondary barriers placed in this manner, most of the antiatoms with trajectories resulting in annihilations within the portion of the region $R - \zeta \leq r \leq R$ would then annihilate on the secondary barriers. Thus, the annihilations due to these trajectories could be distinguished from those occurring just outside of the shadow region.

Prior studies on aperture-based antihydrogen gravity experiments considered the use of a horizontal drift tube, which was intended to be compatible with the ALPHA apparatus. The present work proceeded without regard to compatibility with an existing experimental setup, and a new apparatus would be required to employ the configuration considered here. The configuration was chosen with the intent of minimizing the number of antiatoms necessary for an aperture-based experiment to indicate the direction of free fall acceleration of antimatter. However, it was assumed that antihy-

drogen can be produced within an antiproton plasma at a temperature of 4 K. The assumption is significant, because an antiproton plasma has never been cooled to a temperature significantly lower than 4 K.

In summary: An analytical model and a Monte Carlo simulation have been developed of an antihydrogen gravity experiment with parallel plate geometry. Calculations show that for the parameters considered, a minimum of about 100,000 antiatoms would have to be produced for the associated annihilation distribution to begin to indicate the direction of acceleration of antihydrogen due to gravity. The analysis indicates that a substantial reduction in the minimum number of synthesized antiatoms may be possible relative to that predicted by the previous studies of the aperture-based approach. The present study for a parallel plate geometry also indicates that it is advantageous: (1) to use plates with large radii so that the shadow region can be larger, (2) to use small-radius barriers that form an aperture close to the antihydrogen production region, (3) to use an optimized separation distance between the top and bottom plates, (4) to produce antihydrogen at a low temperature and (5) to produce antihydrogen in a region that is as small as possible.

ACKNOWLEDGMENTS

The authors would like to thank R. Lane and A. Kiester for help with high performance computing. This material is based upon work supported by the Department of Energy under Grant No. DE-FG02-06ER54883 and by the National Science Foundation under Grant No. PHY-1202428.

APPENDIX

The expressions given by Eq. (21) are arrived at as follows: Each antiatom is considered to have initial coordinates equally likely to be located anywhere within a spheroidal volume centered at the origin. An initial z coordinate is randomly selected from within the length of the spheroid using $z_0 = \eta_z L_p/2$. Next, using the equation of the ellipse traced out by the spheroid in the r-z plane,

$$1 = \left(\frac{r}{\rho_p}\right)^2 + \left(\frac{2z}{L_p}\right)^2, \tag{A1}$$

an expression for the maximal radial distance from the z-axis is obtained by evaluating Eq. (A1) at $z = z_0$ and $r = r_{\max}$, and then solving for $r_{\max}$:

$$r_{\max} = \rho_p \sqrt{1 - \left(\frac{2z_0}{L_p}\right)^2}. \tag{A2}$$

The sampling expressions for the radial and azimuthal cylindrical coordinates are $r_0 = r_{\max}\sqrt{R_r}$ and $\Phi_0 = 2\pi R_\phi$. Thus, the sampling expressions for the associated Cartesian components are given by $x_0 = r_0 \cos(\Phi_0)$ and $y_0 = r_0 \sin(\Phi_0)$.

Due to the finite dimensions of the antihydrogen source, there exists a problem in determining the radial distance b from the z-axis at which the barriers should be placed. This issue is addressed by noting that the extent of the shadow region R is determined by high energy antiatoms that have initial coordinates on the surface of the spheroid and have trajectories that pass infinitesimally close to the edge of each barrier. Such an antiatom will trace out a roughly linear trajectory that may be represented as the equation of the tangent line to the ellipse in the r-z plane. Also, a straight line trajectory that starts at $z > 0$ passes through the point $r = R$ and $z = -Z$. Written in terms of a few constants, the final result is given by

$$b = \frac{-a + Z + \alpha R}{\alpha}. \tag{A3}$$

Here,

$$\alpha = \frac{L_p c_1 c_3}{2\rho_p^2 [2Z(\rho_p L_p)^2 - c_2]} \tag{A4}$$

where

$$c_1 = (L_p R)^2 + (2Z\rho_p)^2,$$
$$c_2 = L_p^2 R\sqrt{L_p^2(R^2 - \rho_p^2) + 4Z^2\rho_p^2},$$
$$c_3 = \rho_p L_p\sqrt{1 - \left(\frac{c_2 - 2Z(L_p\rho_p)^2}{L_p c_1}\right)^2}. \tag{A5}$$

To obtain this result, the equation of the tangent line is written in general form as

$$z = \alpha r + \beta, \tag{A6}$$

where α and β are the slope and z-intercept of the tangent line, respectively. The slope of the tangent line evaluated at some point on the ellipse, $r = r_i$ and $z = z_i$, is found by implicitly differentiating Eq. (A1) with respect to r and solving for $\alpha = \frac{dz}{dr}$. Doing so yields

$$\alpha = -\frac{r_i L_p^2}{4z_i\rho_p^2}. \tag{A7}$$

The slope of the line passing through the points $P_1 = (r_i, z_i)$ and $P_2 = (R, -Z)$ is also given by

$$\alpha = \frac{z_i + Z}{r_i - R}. \tag{A8}$$

An expression for r_i in terms of z_i is obtained by evaluating Eq. (A1) at $r = r_i$, $z = z_i$ and solving for r_i,

$$r_i = \rho_p\sqrt{1 - \left(\frac{2z_i}{L_p}\right)^2}. \tag{A9}$$

Substituting this result into Eqs. (A7) and (A8), setting the two equations equal and solving for z_i yields an expression for z_i in terms of R, Z, L_p and ρ_p. Using Eq. (A9), the slope α may then be written in the form of Eq. (A4). To find the z-intercept β, Eq. (A6) is evaluated at $P_2 = (R, -Z)$ and solved yielding

$$\beta = -(\alpha R + Z). \tag{A10}$$

Equation (A6) may then be written as

$$z = \alpha(r - R) - Z. \tag{A11}$$

Finally, to obtain b, Eq. (A11) is evaluated at $r = b$ and $z = -a$ and solved yielding Eq. (A3).

[1] G. B. Andresen, M. D. Ashkezari, M. Baquero-Ruiz, W. Bertsche, P. D. Bowe, E. Butler, C. L. Cesar, S. Chapman, M. Charlton, A. Deller, S. Eriksson, J. Fajans, T. Friesen, M. C. Fujiwara, D. R. Gill, A. Gutierrez, J. S. Hangst, W. N. Hardy, M. E. Hayden, A. J. Humphries, R. Hydomako, M. J. Jenkins, S. Jonsell, L. V. Jorgensen, L. Kurchaninov, N. Madsen, S. Menary, P. Nolan, K. Olchanski, A. Olin, A. Povilus, P. Pusa, F. Robicheaux, E. Sarid, S. Seif el Nasr, D. M. Silveira, C. So, J. W. Storey, R. I. Thompson, D. P. van der Werf, J. S. Wurtele, and Y. Yamazaki, Nature (London) **468**, 673 (2010).
[2] G. B. Andresen, M. D. Ashkezari, M. Baquero-Ruiz, W. Bertsche, P. D. Bowe, E. Butler, C. L. Cesar, M. Charlton, A. Deller, S. Eriksson, J. Fajans, T. Friesen, M. C. Fujiwara, D. R. Gill, A. Gutierrez, J. S. Hangst, W. N. Hardy, R. S. Hayano, M. E. Hayden, A. J. Humphries, R. Hydomako, S. Jonsell, S. L. Kemp, L. Kurchaninov, N. Madsen, S. Menary, P. Nolan, K. Olchanski, A. Olin, P. Pusa, C. O. Rasmussen, F. Robicheaux, E. Sarid, D. M. Silveira, C. So, J. W. Storey, R. I. Thompson, D. P. van der Werf, J. S. Wurtele, and Y. Yamazaki, Nature Physics **7**, 558 (2011).
[3] C. Amole, M. D. Ashkezari, M. Baquero-Ruiz, W. Bertsche, E. Butler, A. Capra, C. L. Cesar, M. Charlton, A. Deller, S. Eriksson, J. Fajans, T. Friesen, M. C. Fujiwara, D. R. Gill, A. Gutierrez, J. S. Hangst, W. N. Hardy, M. E. Hayden, C. A. Isaac, S. Jonsell, L. Kurchaninov, A. Little, N. Madsen, J. T. K. McKenna, S. Menary, S. C. Napoli, K. Olchanski, A. Olin, P. Pusa, C. O. Rasmussen, F. Robicheaux, E. Sarid, C. R. Shields, D. M. Silveira, C. So, S. Stracka, R. I. Thompson, D. P. van der Werf, J. S. Wurtele, A. Zhmoginov, and L. Friedland, Physics of Plasmas **20**, 043510 (2013).
[4] C. Amole, M. D. Ashkezari, M. Baquero-Ruiz, W. Bertsche, E. Butler, A. Capra, C. L. Cesar, M. Charlton, S. Eriksson, J. Fajans, T. Friesen, M. C. Fujiwara, D. R. Gill, A. Gutierrez, J. S. Hangst, W. N. Hardy, M. E. Hayden, C. A. Isaac, S. Jonsell, L. Kurchaninov, A. Little, N. Madsen, J. T. K. McKenna, S. Menary, S. C. Napoli, P. Nolan, A. Olin, P. Pusa, C. O. Rasmussen, F. Robicheaux, E. Sarid, D. M. Silveira, C. So, R. I. Thompson, D. P. van der Werf, J. S. Wurtele, A. I. Zhmoginov, and A. E. Charman, Nature Communications **4**, 1785 (2013).

[5] G. Gabrielse, W. S. Kolthammer, R. McConnell, P. Richerme, R. Kalra, E. Novitski, D. Grzonka, W. Oelert, T. Sefzick, M. Zielinski, D. Fitzakerley, M. C. George, E. A. Hessels, C. H. Storry, M. Weel, A. Mullers, and J. Walz, Physical Review Letters **106**, 073002 (2011).
[6] G. Gabrielse, R. Kalra, W. S. Kolthammer, R. McConnell, P. Richerme, D. Grzonka, W. Oelert, T. Sefzick, M. Zielinski, D. W. Fitzakerley, M. C. George, E. A. Hessels, C. H. Storry, M. Weel, A. Mullers, and J. Walz, Physical Review Letters **108**, 113002 (2012).
[7] P. Richerme, G. Gabrielse, S. Ettenauer, R. Kalra, E. Tardiff, D. W. Fitzakerley, M. C. George, E. A. Hessels, C. H. Storry, M. Weel, A. Mullers, and J. Walz, Physical Review A **87**, 023422 (2013).
[8] A. Mohri and Y. Yamazaki, EPL (Europhysics Letters) **63**, 207 (2003).
[9] Y. Enomoto, N. Kuroda, K. Michishio, C. H. Kim, H. Higaki, Y. Nagata, Y. Kanai, H. A. Torii, M. Corradini, M. Leali, E. Lodi-Rizzini, V. Mascagna, L. Venturelli, N. Zurlo, K. Fujii, M. Ohtsuka, K. Tanaka, H. Imao, Y. Nagashima, Y. Matsuda, B. Juhász, A. Mohri, and Y. Yamazaki, Physical Review Letters **105**, 243401 (2010).
[10] D. Krasnicky, S. Aghion, C. Amsler, A. Ariga, T. Ariga, A. S. Belov, G. Bonomi, P. Braunig, R. S. Brusa, J. Bremer, G. Burghart, L. Cabaret, M. Caccia, C. Canali, R. Caravita, F. Castelli, G. Cerchiari, S. Cialdi, D. Comparat, G. Consolati, L. Dassa, S. Di Domizio, L. Di Noto, M. Doser, A. Dudarev, A. Ereditato, R. Ferragut, A. Fontana, P. Genova, M. Giammarchi, A. Gligorova, S. N. Gninenko, S. D. Hogan, S. Haider, E. Jordan, L. V. Jorgensen, T. Kaltenbacher, J. Kawada, A. Kellerbauer, M. Kimura, V. Lagomarsino, S. Mariazzi, V. A. Matveev, F. Merkt, F. Moia, G. Nebbia, P. Nedelec, M. K. Oberthaler, N. Pacifico, V. Petracek, C. Pistillo, F. Prelz, M. Prevedelli, C. Regenfus, C. Riccardi, O. Rohne, A. Rotondi, H. Sandaker, P. Scampoli, J. Storey, M. A. Subieta Vasquez, M. Spacek, G. Testera, R. Vaccarone, F. Villa, and S. Zavatarelli, AIP Conference Proceedings **1521**, 144 (2013).
[11] P. Perez and Y. Sacquin, Classical and Quantum Gravity **29**, 184008 (2012).
[12] F. Robicheaux, Journal of Physics B: Atomic, Molecular and Optical Physics **41**, 192001 (2008).
[13] G. Gabrielse, Advances in Atomic, Molecular, and Optical Physics **50**, 155 (2005).
[14] M. Charlton, J. Eades, D. Horvath, R. J. Hughes, and C. Zimmermann, Physics Reports **241**, 65 (1994).
[15] M. H. Holzscheiter, M. Charlton, and M. M. Nieto, Physics Reports **402**, 1 (2004).
[16] C. M. Surko and R. G. Greaves, Physics of Plasmas **11**, 2333 (2004).
[17] N. Madsen, Philosophical Transactions of the Royal Society A **368**, 3671 (2010).
[18] C. A. Ordonez and R. M. Hedlof, AIP Advances **2**, 012176 (2012).
[19] R. M. Hedlof and C. A. Ordonez, AIP Conference Proceedings **1525**, 102 (2013).